Global ocean surface carbon product

Thi Tuyet Trang Chau, Marion Gehlen, Frédéric Chevallier

Copernicus Marine Service

QUALITY INFORMATION DOCUMENT

Multi Observation Production Centre

Global Ocean Surface Carbon Product

MULTIOBS_GLO_BIO_CARBON_SURFACE_REP_015_008

Issue: 5.0

Contributors: T. T. Trang Chau, Marion Gehlen, Frédéric Chevallier

Approval date by the CMEMS product quality coordination team: 12/12/2023

CHANGE RECORD

When the quality of the products changes, the QuID is updated and a row is added to this table. The third column specifies which sections or sub-sections have been updated. The fourth column should mention the version of the product to which the change applies.

Issue	Date	§	Description of Change	Author	Validated by
0.0	2019/01	All	Creation of the document	Marion Gehlen, Thi Tuyet Trang Chau	Mercator Ocean
1.0	2019/12	All	Update of the description: new methods (reconstruction and uncertainty quantification) and the corresponding validation	Thi Tuyet Trang Chau, Marion Gehlen, Frédéric Chevallier	Mercator Ocean
2.0	2020/09	All	Update of the description and validation results corresponding to changes in: • input fields in reconstruction of surface ocean partial pressure of carbon dioxide, • parameterization of surface ocean downward mass flux of carbon dioxide (Wanninkhof 2014 instead of Wanninkhof 1992), uncertainty quantification of surface ocean pH.	Thi Tuyet Trang Chau, Marion Gehlen, Frédéric Chevallier	Stéphanie Guinehut
3.0	2021/09	All	Update of the description and validation results corresponding to extensions of data coverage: • spatial extension towards the coasts and high latitudes (above 60°N) • temporal extension for the year 2020	Thi Tuyet Trang Chau, Marion Gehlen, Frédéric Chevallier	Stéphanie Guinehut
3.1	2022/06	all	New template	Thi Tuyet Trang Chau, Marion Gehlen, Frédéric Chevallier	S. Mulet
4.0	2022/09	all	Update of the description and validation results corresponding to: ● update of input data, ● addition of new variables (total alkalinity, dissolved inorganic carbon, saturation state with respect to calcite and aragonite), ● temporal extension for the year 2021, ● changes in units of surface ocean partial pressure of carbon dioxide spco2 (from Pa to µatm) and of surface ocean downward mass flux of carbon dioxide fgco2 (from kg m-2 s-1 to molC m-2 yr-1).	Thi Tuyet Trang Chau, Marion Gehlen, Frédéric Chevallier	S. Mulet

Issue	Date	§	Description of Change	Author	Validated by
5.0	2023/09	all	Update of the description and validation results corresponding to: ● update of input fields, ● increase of spatial resolution (1° to 0.25°), ● temporal extension for the year 2022.	Thi Tuyet Trang Chau, Marion Gehlen, Frédéric Chevallier	H. Etienne

Table of contents

I EXECUTIVE SUMMARY

I.1 Products covered by this document

This document presents the approaches and tools used to produce and validate the Global Ocean Surface Carbon Product **MULTIOBS_GLO_BIO_CARBON_SURFACE_REP_015_008**.

Short Description	Product code	Area	Delivery Time
Surface Carbon	MULTIOBS_GLO_BIO_CARBON_SURFACE_REP_015_008	Global	Yearly

The product provides a data set of ocean surface carbon variables on a regular grid (0.25°x0.25°) with a monthly resolution from 1985 onward. These variables are (1) spco2 - surface ocean partial pressure of carbon dioxide, (2) fgco2 - surface ocean downward mass flux of carbon dioxide expressed as carbon (positive for flux into the ocean), (3) ph - surface pH, (4) talk - total alkalinity in surface seawater, (5) tco2 - surface ocean dissolved inorganic carbon, (6) omega_ca - saturation state of surface seawater with respect to calcite, and (7) omega_ar - saturation state of surface seawater with respect to aragonite.

I.2 Summary of the results

Surface ocean partial pressure of carbon dioxide **(spco2 [µatm])**

Surface ocean partial pressure of CO_2 is obtained from an ensemble of Feed Forward Neural Networks (FFNNs) which is referred to as CMEMS-LSCE-FFNNv2 (Chau et al., 2022; 2023). The models were trained on 100 subsampled datasets from the Surface Ocean CO_2 Atlas (SOCAT) (https://www.socat.info/, last access: 20/06/2023). Sea surface salinity, temperature, sea surface height, mixed layer depth, atmospheric CO_2 mole fraction, chlorophyll, spco2 climatology, latitude and longitude are used as predictors (Table 2 in Section II).

The CMEMS-LSCE-FFNNv2 approach follows a leave-***p***-out cross-validation (***p*** spco2 observations corresponding to the month of reconstruction are excluded from the training data), allowing the quality of the reconstruction to be assessed against independent SOCAT data. At the global scale and over the full period of reconstruction (1985-2022), the root-mean-square difference (RMSD) is ~18.0 µatm (open ocean: 14.3 µatm, coastal: 28.6 µatm) and the coefficient of determination (r^2) is 0.81 (open ocean: 0.83, coastal: 0.73). CMEMS-LSCE-FFNNv2 quantifies spatial and temporal model uncertainties in terms of standard deviations of the 100-member ensembles.

The SOCAT database is an extensive compilation of measurements of near-surface CO2 fugacity made from a variety of observing platforms and instruments (Bakker et al., 2016). The period covered by the reconstruction corresponds to a percentage larger than 85% of that data set. As shown in Figure 2, the spatial distribution of observations is, however, very heterogeneous and the data density remains poor over large areas of the global ocean (e.g., large areas of the Pacific Ocean, Indian Ocean) or seasonally biased (high latitudes). The approach ensures an optimal usage of available data but remains sensitive to data density.

Surface ocean downward mass flux of carbon dioxide **(fgco2 [molC m-2 yr-1])**

The flux of CO_2 was estimated using the gas exchange formulation

$$\mathrm{fgco2} = -k\rho L(1-f_{\text{sea ice}})(\mathrm{spco2}-\mathrm{apco2}) \quad \text{Eq. (1)},$$

where k is the gas transfer velocity (or piston velocity), ρ is the seawater density, L is the temperature-dependent solubility of CO_2, $f_{\text{sea ice}}$ is the sea ice fraction, and apco2 is the atmospheric partial pressure of CO_2.

The global ocean CO_2 sink corresponds to the global integral of fgco2 over space and time. In 2022 [resp. 2021], the global ocean CO_2 sink was 2.49±0.13 [resp. 2.54±0.11] PgC/yr (Figure 1 and Table 4). The number behind the ± sign corresponds to the standard deviation (σ) computed from the ensemble and it is thus an estimate of the uncertainty associated with the reconstruction. The average over the full period 1985-2022 is 1.79±0.10 PgC/yr with an interannual variability (temporal standard deviation) of 0.45 PgC/yr. Taking into account the total ocean area of 361.9e6 km^2 and the outgassing of river carbon of 0.65 PgC/yr (Regnier et al., 2022) yields an anthropogenic carbon uptake by the ocean of 3.23±0.13 PgC/yr [3.28±0.11 PgC/yr] for 2022 [2021], and 2.51±0.10 PgC/yr averaged over the years 1985-2022. Our data-based estimates of the anthropogenic fluxes are in line with the estimates in Global Carbon Budget 2022 (GCB2022) by Friedlingstein et al. (2022) (see Table 4).

Surface ocean pH on total scale **(ph [-]),** ***total alkalinity*** **(talk [µmol kg-1]),** ***dissolved inorganic carbon*** **(tco2 [µmol kg-1]), and** ***saturation state with respect to calcite*** **(omega_ca [-])** ***and aragonite*** **(omega_ar [-])**

Time- and space-varying alkalinity fields were obtained from a multivariate linear regression (LIAR, Carter et al., 2016, 2018) with salinity, temperature, dissolved silica and nitrate (Table 2, Section II) used as independent variables. Surface ocean pH, dissolved inorganic carbon (DIC), and saturation state of seawater with respect to calcite and aragonite were computed from the reconstructed spco2, and reconstructed surface ocean alkalinity using the CO2sys speciation software (Van Heuven et al., 2011; Lewis and Wallace, 1998). Uncertainty of pH, total alkalinity, DIC, and saturation state at each grid cell and time step is derived from LIAR and CO2sys error propagation of their input fields' uncertainties.

The reconstructed alkalinity, DIC, and pH have been assessed with GLODAPv2.2022 bottle data. This product provides direct measurements of alkalinity, DIC, and pH.

For the period 1985-2021, CMEMS-LSCE results in open-ocean alkalinity [DIC] estimates with an RMSD of 22.2[22.6] µmol kg^{-1}, and an r^2 value of 0.90 [0.91]. The coastal reconstruction of these two variables is much less skillful than the open ocean (Table 1). The global error between pH from GLODAPv2.2022 bottle data and the reconstructed pH over the period 1985-2021 is 0.039 pH units for RMSD (open: 0.029, coastal: 0.046), and the r^2 value is 0.54 (open: 0.70, coastal: 0.45). pH decreases in response to the uptake of CO_2 by the ocean. The rate of decrease computed over the period of reconstruction is 0.017±0.002 pH units per decade (Figure 1).

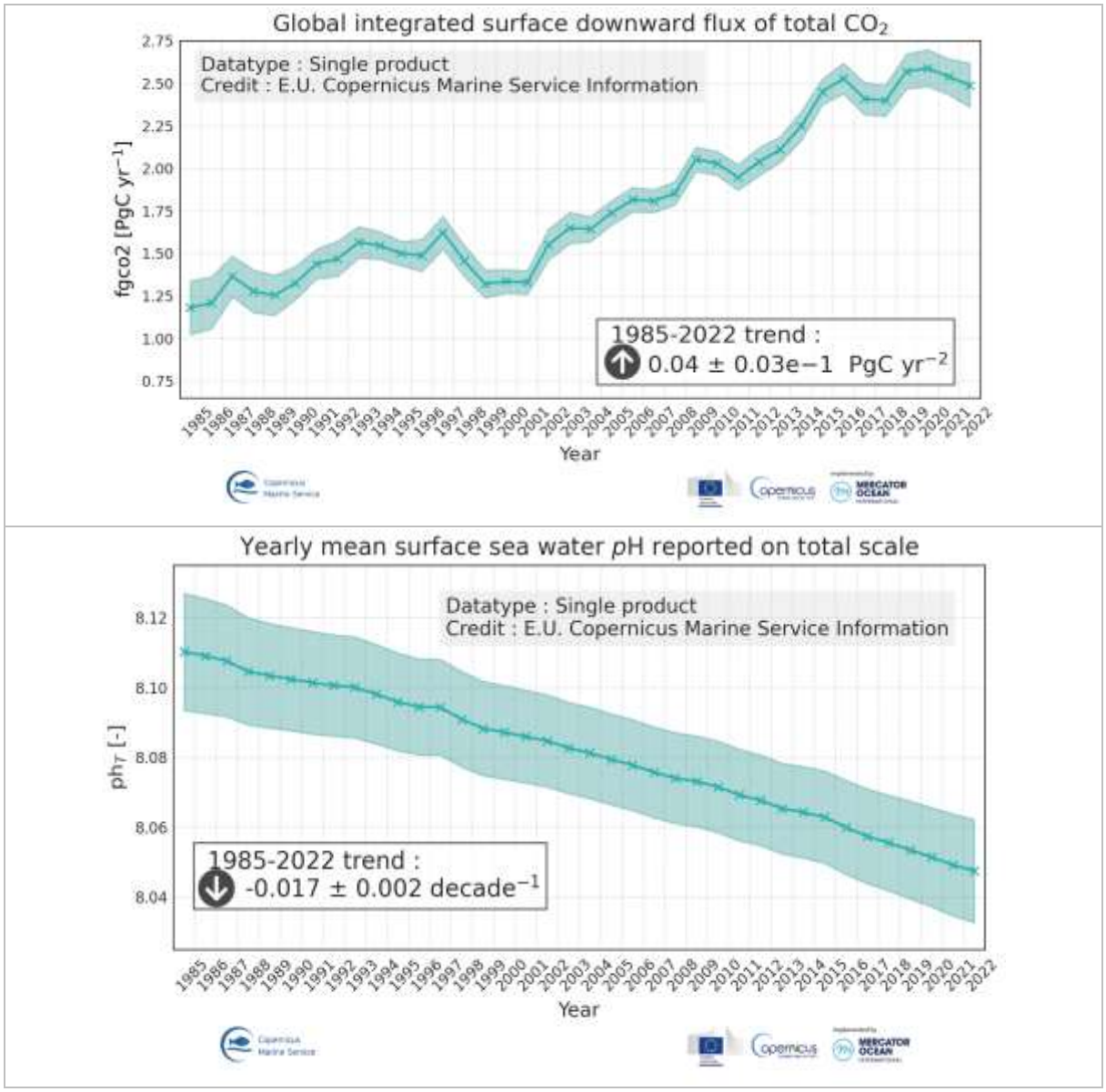

Figure 1. Top: area integrated yearly surface downward flux of total CO2 for the period from 1985 to 2022 (GLOBAL_OMI_HEALTH_CARBON_co2_flux_integrated product). Bottom: yearly mean surface pH reported on total scale (GLOBAL_OMI_HEALTH_CARBON_ph_area_averaged CMEMS product). The uncertainty envelop is defined as the 68% confidence interval (estimate ± uncertainty) of yearly means. Trend and uncertainty are defined as the slope and its residual standard deviation estimated with a linear least-squares regression.

I.3 Estimated Accuracy Numbers

The quality of the reconstruction is assessed against independent SOCAT data in a leave-*p*-out cross-validation where *p* spco2 observations corresponding to a given month of reconstruction have been excluded from the training data. A ratio of 2:1 for training and validating is used. At the global scale and over the full period of reconstruction (1985-2022), the main statistics are reported in table 1.

For total alkalinity, DIC, and pH, the statistics are with respect to the independent GLODAPv2.2022 bottle data over the period 1985-2022 (https://glodap.info/index.php/merged-and-adjusted-data-product-v2-2022/: last access 2023/07/31).).

Table 1: Estimated skill over the open (O), and coastal (C) oceans. MAD = Mean Absolute Deviation, RMSD = Root Mean Square Deviation, r^2 = coefficient of determination (see section III for definitions).

Variable		Metrics			Units
		MAD	RMSD	r^2	
spco2	(O)	9.7	14.3	0.83	µatm
	(C)	18.0	28.6	0.73	
talk	(O)	10.8	22.1	0.90	µmol kg^{-1}
	(C)	42.5	83.4	0.71	
tco2	(O)	11.68	22.63	0.91	µmol kg^{-1}
	(C)	40.82	73.33	0.91	
ph	(O)	0.013	0.022	0.70	pH total scale
	(C)	0.035	0.060	0.45	

II PRODUCTION SYSTEM DESCRIPTION

Production centres name: Laboratoire des Sciences du Climat et de l'Environnement (LSCE) (MULTIOBS-LSCE-GIF-FR)

Production system name: CMEMS-LSCE

II.1 Origin of input fields

In addition to the predictors listed in Table 2, latitude and longitude are also used as predictors for the reconstruction of surface ocean pCO_2.

Table 2: Details of input fields

Reconstruction of surface ocean CO_2 partial pressure		
Target data: surface ocean CO_2 partial pressure.		
Measurements of CO_2 fugacity	Bakker et al., 2016; 2023	SOCAT 2023 (last access 20/06/2023)
Predictor data		
Sea surface temperature	Good et al. 2020	CMEMS: SST_GLO_SST_L4_REP_OBSERVATIONS_010_011 (1985-2021) SST_GLO_SST_L4_NRT_OBSERVATIONS_010_001 (2022)
Sea surface salinity	Buongiorno Nardelli et al. 2016; Droghei et al. 2016, 2018	CMEMS: MULTIOBS_GLO_PHY_S_SURFACE_MYNRT_015_013 (1993-2022) Climatology (1985-1992) computed from the available data (1993-2022)
Sea surface height	CLS-TOULOUSE	CMEMS: SEALEVEL_GLO_PHY_L4_MY_008_047 (1993-2021) SEALEVEL_GLO_PHY_L4_NRT_OBSERVATIONS_008_046 (2022) Climatology plus linear trend (1985-1992) computed from the available data (1993-2022)
Mixed layer depth	Menemenlis et al., 2008	ECCO2: "Estimating the Circulation and Climate of the Ocean" project Phase II (1992-2022) Climatology (1985-1991) computed from the available data (1992-1997)
Chlorophyll	GlobColour	CMEMS:OCEANCOLOUR_GLO_BGC_L4_MY_009_104 (1998-2022) Climatology computed from the available data (1985-1997)
Atmospheric CO_2 mole fraction	Chevallier et al. 2005, 2010; Chevallier, 2013	CO_2 atmospheric inversion from the Copernicus Atmosphere Monitoring Service Surface: v21r1 (1985-2021) Satellite: v22r1 (2022)
spco2 climatology	Takahashi et al. (2009)	LDEO spco2 climatology

Reconstruction of surface ocean downward mass flux of CO_2		
6-hourly wind speed Total pressure	Hersbach et al. 2018	ERA5 hourly data on single levels from 1959 to present
Atmospheric CO2 mole fraction	Chevallier et al. 2005, 2010; Chevallier, 2013	CO2 atmospheric inversion from the Copernicus Atmosphere Monitoring Service (https://atmosphere.copernicus.eu/)
Sea ice fraction	Good et al. 2020	CMEMS SST_GLO_SST_L4_REP_OBSERVATIONS_010_011 (1985-2021) SST_GLO_SST_L4_NRT_OBSERVATIONS_010_001 (2022)

Reconstruction of surface ocean pH on total scale		
Nitrate Silicate Phosphate	Garcia et al. 2019	World Ocean Atlas 2018
Alkalinity, DIC, pH (validation data)	Lauvset et al 2022	GLODAPv2.2022 bottle data

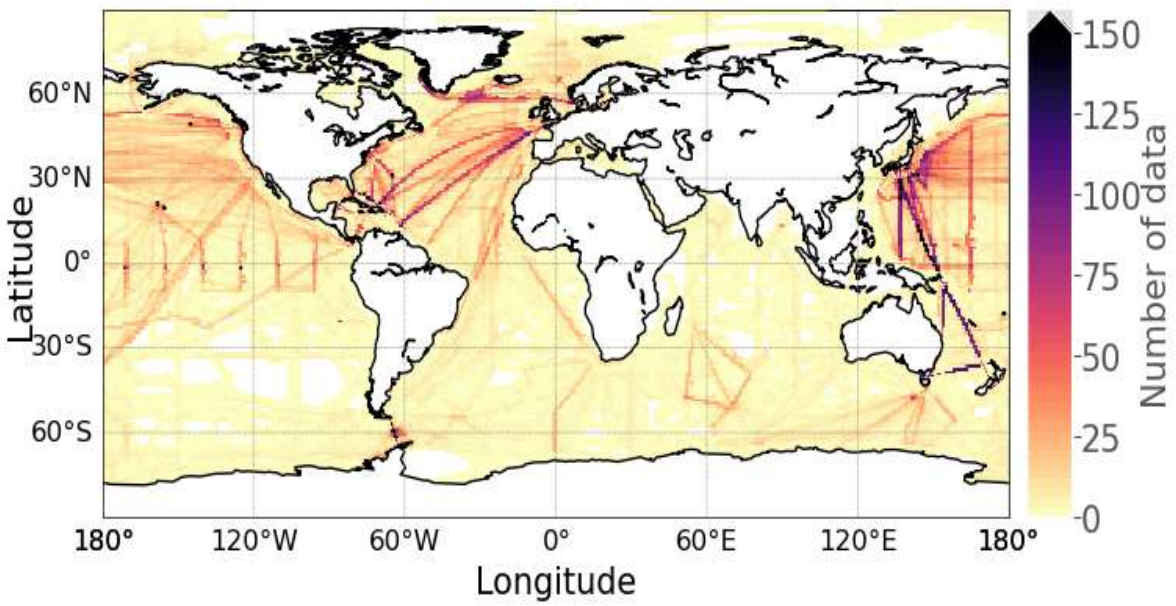

*Figure 2 Distribution of SOCAT v2023 – ship traces for the period Jan 1985-Dec 2022 (Bakker et al., 2023): **amount** of monthly data on $0.25^{o}\times0.25^{o}$ regular grid. A combination of the original 0.25°-coastal-ocean datasets and the 1°-open-ocean datasets downscaled to **a** resolution **of 0.25°×0.25°** is used in model fitting (see Sect. II.2).*

II.2 Description of system

(a) Reconstruction of surface ocean carbon dioxide partial pressure

Central to the production process is the reconstruction of surface ocean carbon dioxide partial pressure (spco2) by a Feed Forward Neural Network (FFNN) model following an ensemble-based approach (Chau et al. 2022, 2023). The ensemble network was developed at the *Laboratoire des Sciences du Climat et de l'Environnement* (LSCE) and validated as an improvement of LSCE-FFNN-v1 by Denvil-Sommer et al. (2019), see Chau et al. (2020) for intercomparison. The model outputs are part of the Copernicus Marine Environment Monitoring Service (CMEMS). It is hence referred to as CMEMS-LSCE-FFNNv2.

Taking advantage of the Surface Ocean CO_2 Atlas (SOCAT) (Bakker et al., 2016), the ensemble-based FFNN approach was first used to reconstruct the global distribution of spco2 with a monthly resolution over the global 1°×1°-gridded surface ocean (Chau et al, 2022). Since the year 2023, an extension proposed by Chau et al. (2023) is adopted to map spco2 to the global surface ocean with a 16-fold increase in spatial resolution. SOCAT provides the two monthly, gridded products: one covers the global ocean at 1° spatial resolution, and another includes coastal data on 0.25°-grid cells. To fit FFNNs, we create a global dataset of spco2 at monthly, 0.25° resolutions (Chau et al., 2023) by combining the original coastal SOCAT dataset and a 0.25°-open-ocean dataset. The latter is a downscaled version of the 1°-open-ocean product wherein its data are duplicated conservatively for sixteen 0.25°-subgrid cells.

FFNN models were fitted on 100 datasets sub-sampled randomly from the drivers and SOCAT data with a ratio of 2:1 for training and validation. The model is sensitive to the observational coverage. This limitation is partly overcome by the FFNN approach as the reconstruction of monthly global ocean distributions draws on a larger data set such that FFNN outputs remain close to realistic values. The approach further uses observations in a 3-month gliding window centered on the month of reconstruction. Note that the data from the month of reconstruction is excluded from the training data in order to reduce model overfitting.

The means (μ) and standard deviations (σ) are computed from the 100-member ensembles of surface ocean partial pressure of CO_2 reconstructions, as well as surface ocean downward mass flux of CO_2. The standard deviation stands for the associated model uncertainty. In this report, the notation $\mu \pm \sigma$ expresses a best estimate of the surface ocean partial pressure of CO_2. along with its relative uncertainty. An identical ensemble-based approach is applied to the other carbon variables (pH, total alkalinity, dissolved inorganic carbon, and saturation state with respect to calcite and aragonite). In cases of the uncertainty reported for the temporal mean of carbon variables (e.g., Figures 4, 6, 7, and 8), we define its representative estimate as follows

$$\sigma_{ij} = \{ \Sigma_m [\Sigma_t (x_{t,ij}^m - x_{t,ij})^2] / (100\ T) \}^{1/2} \quad \text{(Eq. 2)},$$

where $x_{t,ij}^m$ is a member estimate of each variable in the surface carbon product at the ij^{th} 0.25°×0.25°-grid box and time step t; and $x_{t,ij} = \Sigma_m x_{t,ij}^m / 100$ is the ensemble mean of $\{x_{t,ij}^m\}_{m=1:100}$. Note that, for pH, total alkalinity, DIC, and saturation state, the uncertainty is derived from carbonate system error propagation (see in Sect. II.2.c). 100-member ensembles of these variables are generated based on their best reconstruction and its uncertainty before applying Eq. (2).

(b) Reconstruction of surface ocean downward mass flux of carbon dioxide expressed as carbon

The surface ocean downward mass flux of CO_2 is computed from the gas exchange formulation (Eq. 1)

$$\mathrm{fgco2} = -k\rho L(1 - f_{\mathrm{sea\ ice}})(\mathrm{spco2} - \mathrm{apco2}),$$

where k is the piston velocity, ρ the seawater density, L is the temperature-dependent solubility of CO_2 (Weiss, 1974), $f_{\text{sea ice}}$ is the sea ice fraction, and apco2 is the atmospheric partial pressure of CO_2. The piston velocity is estimated after Wanninkhof (2014) with wind speed computed from 6-hourly ERA5 wind speed and the sea ice fraction extracted from OSTIA data. spco2 corresponds to the surface ocean pCO_2, reconstructed by the neural network CMEMS-LSCE-FFNNv2 model (Chau et al, 2023) and apco2 was derived from the atmospheric CO_2 mixing ratio fields provided by the CAMS inversion (Chevallier et al. 2005, 2010; Chevallier 2013).

The uncertainty of the surface downward mass flux is quantified after applying the gas exchange formula to the difference between the 100-member ensemble of monthly spco2 estimates and the corresponding apco2 values.

(c) Reconstruction of surface ocean pH, total alkalinity, dissolved inorganic carbon, and saturation state with respect to calcite and aragonite.

Time- and space-varying surface ocean alkalinity fields are obtained from the multivariate linear regression model LIAR (Carter et al., 2016; 2018) as a function of sea surface temperature and salinity, as well as climatological nitrate and dissolved silicate from World Ocean Atlas v2018 (https://www.ncei.noaa.gov/data/oceans/woa/WOA18/). Surface ocean pH, DIC, and the saturation state of sea water with respect to calcite and aragonite are calculated from reconstructed spco2 and talk, temperature, salinity, and nutrients by using the speciation software CO2sys (Van Heuven et al., 2011; Lewis and Wallace, 1998).

Uncertainty of pH, total alkalinity, DIC, and saturation state at each grid cell and time step is derived from LIAR and CO2sys error propagation (Orr et al. 2018). Inputs to the uncertainty propagation routine are default values for dissociation constants while they are space-time varying fields for other variables. Uncertainty estimates for talk and spco2 represent respectively systematic errors from LIAR (Carter et al., 2016; 2018) and randomness errors from the CMEMS-LSCE-FFNNv2 ensemble approach (Chau et al. 2022, 2023). For temperature and salinity, the uncertainties are defined as analysis errors associated with the CMEMS products (Table 2), and for nitrate, silicate, and phosphate climatologies the uncertainties are defined as 15% of the WOA18 data values (see https://archimer.ifremer.fr/doc/00651/76336/77327.pdf).

III VALIDATION FRAMEWORK

III.1 Surface ocean partial pressure of carbon dioxide

Only two thirds of the SOCAT target data are used for the training algorithm, leaving one third for model validation. The models are trained separately for each month, resulting in adaptive models with a common architecture but trained on different data. To increase the amount of data available for training, the models are trained using as target data from a 3-month moving window of the entire period from 1985 onward but excluding the reconstructed month.

Model output is assessed on independent SOCAT data and collocated reconstructed data. A leave-***p***-out cross-validation approach is applied (where ***p*** is the amount of data in the month considered for reconstruction) and 100 random subsamples of independent data are drawn from the SOCAT dataset. The network was run on each subsample. From these 100 results the mean was chosen as an estimate of monthly spco2 per grid cell.

All metrics are computed over the full reconstruction period and the period 1985-2021 for the comparison with the VIprevious release. The assessment is broken down into the five oceanic basins used in data evaluation in the Regional Carbon Cycle Assessment and Processes project – phase 2 (RECCAP2, https://github.com/RECCAP2-ocean/R2-shared-resources/tree/master/data/regions, last access 11/7/2022) (Figure 3). Reconstructed data along the coast are evaluated within the SOCAT coastal zones defined within 400 km from the shoreline and collocated on the 0.25°× 0.25° SOCAT grid5.

III.2 Surface ocean downward mass flux of carbon dioxide

There is no independent data for validating fgco2. CMEMS-LSCE-FFNNv2 estimates of air–sea CO_2 fluxes are assessed by comparison to published estimates derived from an ensemble of global ocean biogeochemical models (GOBMs) and an ensemble of data-based reconstruction models used in the Global Carbon Project (GCP, Friedlingstein et al., 2022). Note that in order to obtain estimates for the anthropogenic fluxes the data-based estimates need to be corrected for the preindustrial outgassing, i.e., of riverine carbon input, of 0.65 PgC/yr (Regnier et al., 2022).

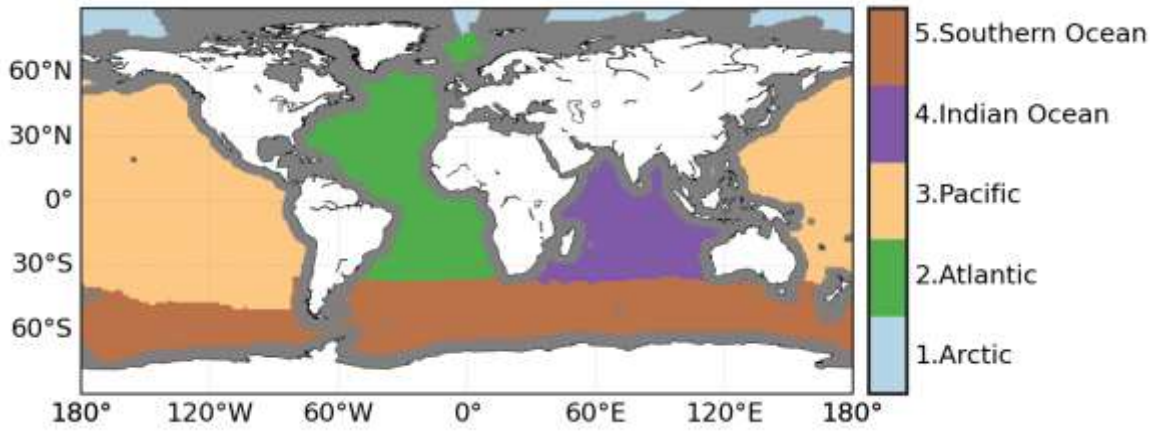

Figure 3. Map of the ocean basins (https://github.com/RECCAP2-ocean/RECCAP2-shared-resources/tree/master/data/regions, last access: 11/7/2022) used for model assessment. The coastal mask (grey) is consistent with the definition of coastal SOCAT coverage (400 km from shoreline; Bakker et al. 2016) collocated on 0.25°×0.25° SOCAT grid.

III.3 Surface ocean pH, total alkalinity, dissolved inorganic carbon, and saturation state with respect to calcite and aragonite

Total alkalinity, DIC, and pH from GLODAPv2.2021 bottle data (https://glodap.info/index.php/merged-and-adjusted-data-product-v2-2022/) are used for the evaluation of reconstructed surface ocean fields during 1985-2021. Only data from depths shallower than 10 m are used. Data are averaged per month and on a regular 0.25°×0.25° grid, which resulted in ~16500 [7500] data points for talk and tco2 [ph] (~38% [28%] distributed along the coastal sector). GLODAP pH data derived from the combination of talk and tco2 data are excluded from our product evaluation. The reconstruction metrics are calculated from co-located reconstructed values at these data points (Table 5 and Figure 9).

IV VALIDATION RESULTS

IV.1 Surface ocean partial pressure of carbon dioxide

Table 3 shows skill scores computed for 5 oceanic regions. It illustrates - for the full period - that the highest RMSDs (open: 30.5 µatm, coastal: 43.93 µatm) and MAD (open: 23.3 µatm, coastal: 30.3 µatm) are associated with the region having the lowest data density and high temporal and/or spatial pCO_2 variations,(Arctic)). The CMEMS-LSCE-FFNNv2 reconstruction over the coastal regions for the full period is roughly twice less effective than over the open ocean in terms of RMSD and MAD overall while it shows a rather good fit with r^2 = 0.73. The high RMSD reflects local high model errors along the continental shelves (Figure 5) which are characterized by complex physical and biological dynamics leading to high variability at small scales. Further model improvement is needed to capture such high spatial and temporal variability of surface ocean spco2 present in observations (see in Bakker et al. 2016; Laruelle et al., 2017, and references therein). An in-depth analysis on the model reconstruction over different oceanic basins for both open and coastal regions is presented in Chau et al. (2022, 2023).

The average surface ocean spco2 for the period 1985-2022 is shown on the left panel of Figure 4. High surface ocean spco2 values are associated to the upwelling of deep water, which is naturally enriched in DIC (Dissolved Inorganic Carbon, e.g., Equatorial Pacific upwelling). Low CO_2 partial pressures are found in cold northern and southern latitudes, a combination of the temperature effect on the solubility of CO_2 and the drawdown of DIC by biological activity. The spatial uncertainty of spco2 corresponding to the standard deviation of outputs from the 100 models from the CMEMS-LSCE-FFNNv2 is displayed on the right panel of Figure 4. These maps illustrate the confidence level in the reconstruction of spco2. Large estimates of the uncertainties were found in the coastal regions, regions sparse or devoid of SOCAT data (see Figure 2) such as Indian Ocean, Southern Ocean, and regions with high or low surface pressure of CO_2 such as East Pacific, Labrador Sea, North Western Pacific.

Table 3: Statistical validation for CMEMS-LSCE-FFNNv2 over the period 1985-2022. Comparison between reconstructed surface ocean spco2 and spco2 values from the SOCAT data that were not used during the algorithm training. Global statistics and regional examples (Figure 3), number of SOCATv2023 data per open (O) and coastal (C) ocean within brackets.

Basins	**Number of data**		**MAD (µatm)**		**RMSD (µatm)**		**r^2**	
	(O)	**(C)**	**(O)**	**(C)**	**(O)**	**(C)**	**(O)**	**(C)**
Global	3413614	508176	9.7	18.0	14.3	28.6	0.83	0.73
Arctic	10695	29387	23.3	30.3	30.7	43.9	0.66	0.53
Atlantic	907433	270554	9.6	16.7	13.7	26.3	0.82	0.78
Pacific	1989418	121944	9.6	17.5	14.5	29.1	0.85	0.69
Indian Ocean	73256	6918	7.5	14.3	10.2	25.7	0.89	0.68
Southern Ocean	432812	79373	10.2	18.8	14.6	28.5	0.68	0.64

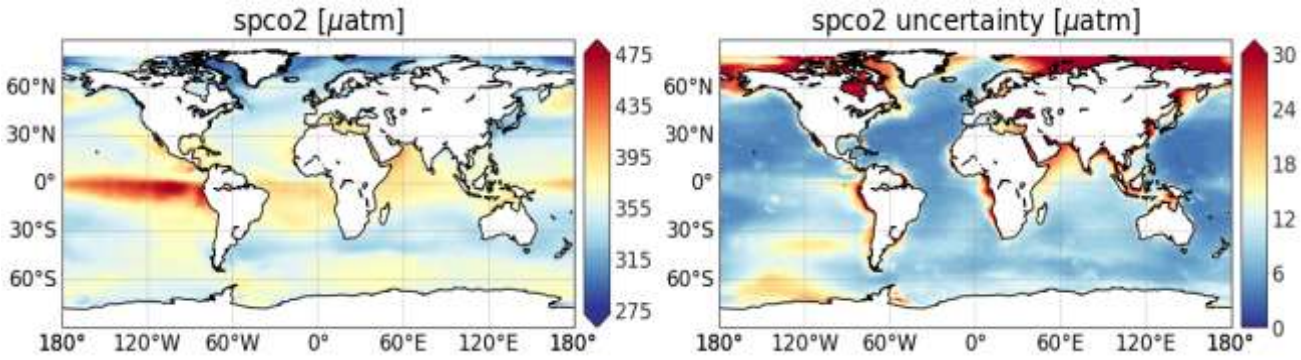

Figure 4. Reconstructed surface ocean carbon dioxide partial pressure averaged over the global ocean for 1985 to 2022. Mean (left) and standard deviation (right) of the 100-member CMEMS-LSCE-FFNNv2 model outputs are shown. The uncertainty estimate of the temporal mean per grid cell is computed following Eq. (2).

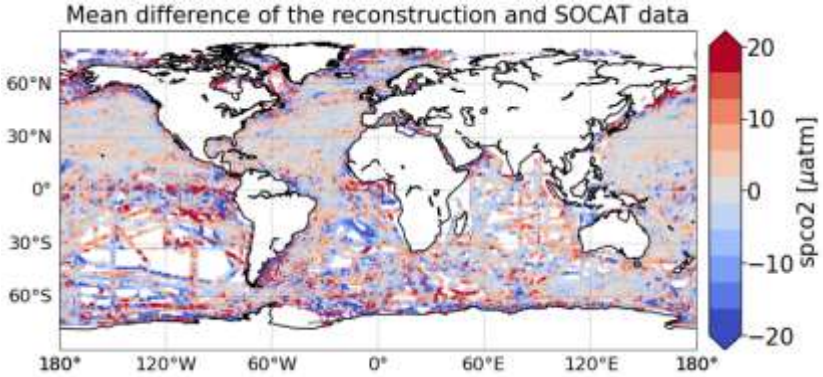

Figure 5. Map of the mean differences between MULTIOBS spco2 and the entire SOCAT dataset [µatm].

While the average bias of reconstructed surface ocean partial pressure compared to the SOCAT data is small, there are areas with persisting strong positive or negative biases (e.g., coastal seas and continental shelves, subpolar and polar regions, Eastern Pacific Ocean, Western South Atlantic). Figure 5 shows the full dataset of the differences from the observations for the period 1985-2022. It hides the still sparse data coverage for individual months, which challenges any reconstruction method. Even more problematic is the poor data coverage of large regions (e.g., coasts, high latitudes, Indian Ocean and South Pacific Ocean). Reconstructed monthly fields are very noisy with high uncertainty over areas with poor data coverage (see Figure 2) and/or high variations of pCO_2, and should be viewed with caution.

IV.2 Surface ocean downward mass flux of carbon dioxide

Table 4 presents a comparison between CMEMS-LSCE and GCB2022 (Global Carbon Budget 2022, Friedlingstein et al. 2022) for the reconstruction of air-sea CO_2 fluxes. The GCB Ocean sinks are the average estimates from an ensemble of global ocean biogeochemical general circulation models (GOBMs) and an ensemble of data-based reconstruction methods.

The global ocean CO_2 sink corresponds to the global integral of fgco2 over space and time. The reconstructed field covers both the open ocean and coastal regions and hence approximately 96.37% of the total ocean area (361.9e6 km^2). In 2022 [resp. 2021], the global ocean CO_2 sink was 2.49±0.13 [resp. 2.54±0.11] PgC/yr (Figure 1). The average of yearly contemporary fluxes over the full period 1985-2022 is 1.79±0.10 PgC/yr with an interannual variability (temporal standard deviation) of 0.45 PgC/yr. Taking into account the total ocean area of 361.9e6 km^2 and the outgassing of river carbon of 0.65 PgC/yr yields an anthropogenic carbon uptake by the ocean of 3.23±0.13 PgC/yr [3.28±0.11 PgC/yr] for 2022 [2021] and 2.51±0.10 PgC/yr for the years 1985-2022. CMEMS-LSCE estimates of the anthropogenic uptake are of similar magnitude as the estimates by Friedlingstein et al. (2022) (see Table 4).

The ensemble-based approach yields spatio-temporal varying uncertainties which are consistent with uncertainty estimates of an ensemble of data-based and model-based approaches in Hauck et al. (2020). However, they are lower than the previous GCB published total estimate of ±0.4 PgC/yr. The latter estimate corresponds to the combination of random uncertainty (ensemble standard deviation of model- and data-based flux estimates) and systematic uncertainty (bias of model-based estimates in anthropogenic carbon cumulation).

*Table 4: Air-sea CO2 flux (PgC/yr) integrated over the global ocean. Comparison between CMEMS-LSCE-FFNNv2 and other estimates for periods in 1985-2022 (*source: Friedlingstein et al. 2022). The estimates of CMEMS-LSCE-FFNNv2 anthropogenic flux were computed by adjusting the contemporary flux estimates with the global ocean area of 361.9e6 km2 and the riverine flux of 0.65 PgC/yr.*

Methods		**Periods**				
		1990s	**2000s**	**2012-2021**	**2021**	**2022**
CMEMS-LSCE-FFNNv2	Contemporary	1.47 ± 0.09	1.68 ± 0.08	2.39 ± 0.09	2.54 ± 0.12	2.49 ± 0.13
	Anthropogenic	2.18 ± 0.09	2.39 ± 0.08	3.13 ± 0.10	3.28 ± 0.11	3.23 ± 0.13
GCB2021*		2.1 ± 0.4	2.3 ± 0.4	2.9 ± 0.4	2.9 ± 0.4	2.9 ± 0.4

The map of average air-sea fluxes of CO_2 for the period 1985-2022 (Figure 6) highlights the regional variability of fluxes over the global ocean (top) and the coastal regions (bottom). Outgassing of CO_2 is associated with the upwelling of CO_2-rich subsurface waters (e.g., Equatorial Pacific). The northern and southern mid to high latitudes are sink regions. The North Atlantic stands out as a major area of CO_2 uptake explained by a marked strong cooling in winter and a vigorous phytoplankton bloom in spring and early summer. A region of enhanced uptake is also associated with the subtropical convergence zone in the southern hemisphere. Based on the gas exchange formulation, the uncertainties derived from the 100-member ensemble of fgco2 estimates can be interpreted as the scalar product of the spco2 uncertainties resulted from the CMEMS-LSCE-FFNNv2 and the gas transfer coefficients ($k\rho L(1-f_{\text{sea ice}})$, from eq. 1). On the right panel of Fig. 6 one notes that the uncertainty for the Southern Ocean, due to its strong and variable winds, is higher than for the other regions.

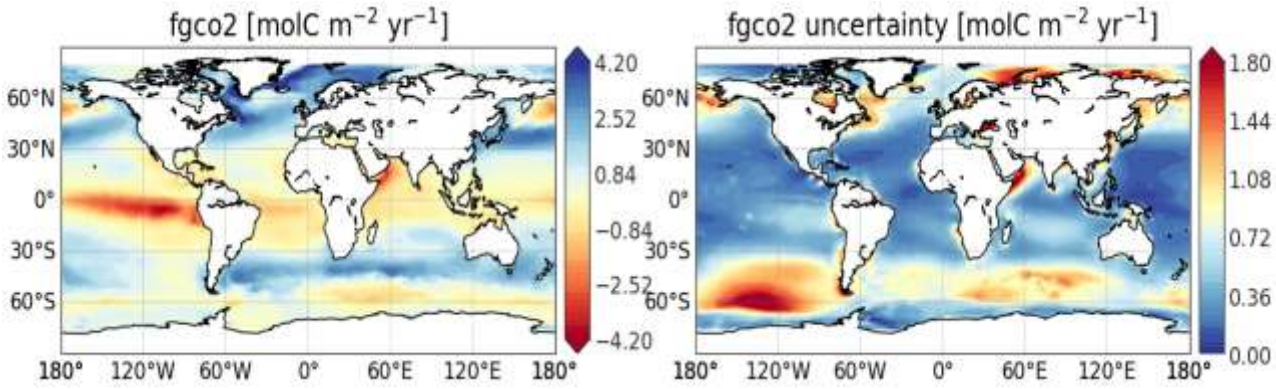

Figure 6. Reconstructed surface downward flux of carbon dioxide averaged over the global ocean for 1985 to 2022. Mean (left, positive values correspond to ocean uptake) and standard deviation (right) computed from the 100-member ensemble of CMEMS-LSCE-FFNNv2 are shown. The uncertainty estimate of the temporal mean per grid cell is computed following Eq. (2).

The global yearly integrated air-sea flux of CO_2 seen in Figure 1 is characterized by interannual variability in response to modes of natural climate variability, which occurs superposed on the trend driven by increasing atmospheric CO_2 levels. The Equatorial Pacific is a dominant source of CO_2 to the atmosphere. Equatorial Pacific outgassing is strongly modulated by ENSO dynamics and imprints global air-sea fluxes of CO_2 (Feely et al., 2010). During El Niño events (e.g., 1997-1998, 2015-2016), reduced upwelling translates into reduced outgassing of CO_2 and an enhanced global ocean net air-sea CO_2 flux. On the contrary, La Niña events (e.g. 2007-2008, 2020-2023) are characterized by increased upwelling, enhanced outgassing and a decreased global ocean net air-sea CO_2 flux (Chau et al. 2022 [Figure 9]).

IV.3 Surface ocean pH, total alkalinity, dissolved inorganic carbon, and saturation state with respect to calcite and aragonite

In comparison with independent measurements from GLODAPv2.2022 over the period 1985-2022, the CMEMS-LSCE-FFNNv2 reconstruction results in open-ocean alkalinity [DIC] with a global MAD of 10.8 [11.7] µmol kg-1, RMSD of 22.2 [22.6] µmol kg-1, and r^2 value of 0.90 [0.91]. Large estimation deviation from GLODAP data is found in high latitudes and tropics. Coastal regions remain challenging for the extrapolation of these carbonate variables with much less model skill and higher uncertainty estimates than those corresponding to the open ocean (Table 5, Figures 7 and 9). However, these model errors and model uncertainties are below 10% of talk or tco2 mean values. The appearance of spikes in the uncertainty maps of surface ocean alkalinity and DIC (Figure 7) as well as of saturation state (Figure 8) are highly correlated to that characterized by the uncertainty field of the CMEMS salinity product (Table 2, Copernicus Marine Data visualization tool for sea surface salinity error.

The assessment of the quality of the CMEMS-LSCE-FFNNv2 reconstruction with respect to pH data from the GLODAPv2.2022 bottle data set yields a global RMSD of 0.022 [0.060] pH and an absolute bias of 0.013 [0.035] pH units over the open [coastal] ocean. Model scores for the regional assessment are shown in Table 5 and Figure 9. CMEMS-LSCE produces reliable estimates of pH over the open ocean between 60°S-60°N. Model errors (Figure 9) and uncertainty estimates (Figure 7) remain high over the coastal seas, continental shelves, and high latitudes. For a comparison with the existing global carbonate product (OceanSODA-ETHZ) over the open ocean, CMEMS-LSCE-FFNNv2 reproduces pH estimates with similar skill scores (Gregor et al. 2021 [Table 3]). This product qualification was based on both GLODAPv2019 and SOCCOM data (direct pH measurements collected by the Southern Ocean Carbon and Climate Observations and Modeling project).

Table 5: Statistical validation for CMEMS-LSCE-FFNNv2 over the period 1985-2022. The assessment is based on the comparison between reconstructed surface ocean data, and GLODAPv2.2022 bottle data set for total alkalinity (talk), DIC (tco2), and pH over the period 1985-2021. Global statistics and regional examples (Figure 3), number of GLODAPv2. 2022 data per open ocean (O) or coastal (C) region between brackets (cont. in next page).

Basins	**talk** [µmol kg^{-1}]							
	Number of data		**MAD**		**RMSD**		**r^2**	
	(O)	**(C)**	**(O)**	**(C)**	**(O)**	**(C)**	**(O)**	**(C)**
Global	10264	6309	10.8	42.5	22.2	83.4	0.90	0.71
Arctic	103	1635	92.8	100.6	106.2	151.0	0.78	0.46
Atlantic	2784	2422	11.7	26.8	30.1	45.9	0.74	0.68
Pacific	4539	1380	9.5	19.7	13.8	28.7	0.91	0.75
Indian Ocean	1177	328	11.2	12.1	15.9	16.4	0.91	0.93
Southern Ocean	1661	544	7.6	13.5	11.0	21.6	0.64	0.56

Table 5 (cont.): Statistical validation for CMEMS-LSCE-FFNNv2 over the period 1985-2022. The assessment is based on the comparison between reconstructed surface ocean data, and GLODAPv2.2022 bottle data set for total alkalinity (talk), DIC (tco2), and pH over the period 1985-2021. Global statistics and regional examples (Figure 3), number of GLODAPv2. 2022 data per open ocean (O) or coastal (C) region between brackets.

Basins	tco2 [µmol kg-1]							
	Number of data		MAD		RMSD		r^2	
	(O)	(C)	(O)	(C)	(O)	(C)	(O)	(C)
Global	10264	6309	11.7	40.8	22.6	73.3	0.91	0.61
Arctic	103	1635	100.8	86.4	112.9	128.5	0.68	0.39
Atlantic	2784	2422	12.3	25.3	28.7	39.7	0.73	0.67
Pacific	4539	1380	10.5	30.5	15.9	44.6	0.92	0.45
Indian Ocean	1177	328	10.6	13.7	14.0	21.8	0.95	0.89
Southern Ocean	1661	544	9.11	16.5	13.0	23.5	0.92	0.79
Basins	**ph[-]**							
	Number of data		MAD		RMSD		r^2	
	(O)	(C)	(O)	(C)	(O)	(C)	(O)	(C)
Global	5411	2080	0.013	0.035	0.022	0.060	0.70	0.45
Arctic	26	300	0.064	0.074	0.107	0.106	0.31	0.48
Atlantic	932	941	0.014	0.029	0.029	0.046	0.58	0.44
Pacific	3222	639	0.013	0.033	0.019	0.057	0.75	0.35
Indian Ocean	551	62	0.009	0.010	0.012	0.013	0.90	0.82
Southern Ocean	680	138	0.014	0.018	0.019	0.024	0.68	0.64

Reconstructed surface ocean alkalinity varies spatially across and between ocean basins. Alkalinity is highest over the tropical Atlantic ocean (Figure 7) in line with high salinity concentration (Copernicus Marine Data visualization tool for sea surface salinity). In the regions where salinity is reduced by precipitation and/or seasonal sea-ice melting (e.g. subpolar Pacific ocean, Arctic river outflows, Equatorial band, Eastern Indian ocean and Indonesian archipelago), surface ocean alkalinity is low. High levels of DIC are reconstructed throughout the Southern Ocean because of upwelling of CO_2 rich waters and subsequent DIC-spreading by prevailing westerlies. Outside of upwelling areas, DIC levels are modulated by biological draw-down and temperature control on CO2 solubility regionally resulting in pronounced seasonal cycles (e.g. subpolar regions, Feely et al. 2001). Uncertainty estimates of the reconstructed alkalinity and DIC are below 5% of the climatological mean values over the open ocean (Figure 7).

Reconstructed saturation states (Ω) with respect to calcite and aragonite (polymorphs of the mineral calcium carbonate, $CaCO_3$) show similar spatial variability across the ocean basins (Figure 8). High values of saturation state with respect to calcite and aragonite are reconstructed over the subtropical and tropical bands (between 30°S-30°N) reflecting relatively high ALK over DIC ratios. A decrease in the saturation state is found in high latitudes and upwelling regions. Lowest values are associated with low alkalinity and high DIC high latitudes waters. While surface waters remain in average oversaturated with

respect to calcite and aragonite (Ω = 1), saturation states below 1.5 are reached locally. Uncertainty estimates for surface ocean saturation state are less than 10% of its global mean, exceptionally for the coastal regions (Figure 8).

Reconstructed surface ocean pH is given on total H^+ scale. Low pH values are found in upwelling regions (e.g., Equatorial Pacific, Arabian Sea) where dissolved inorganic carbon (DIC) enriched subsurface waters reach the surface ocean. Higher values are found in subpolar and polar waters (Figure 7). The uncertainty map of pH displayed on the right plot of Figure 7 is derived through a monthly uncertainty propagation for the 100-ensemble mean and ensemble spread of spco2 following Orr et al. (2018) and the speciation software CO2sys (Lewis and Wallace, 1998; Van Heuven et al., 2011) (see II.2.c for details). Estimates of spco2 and associated uncertainties (see Figure 4) have the largest impact on the estimation of pH uncertainties.

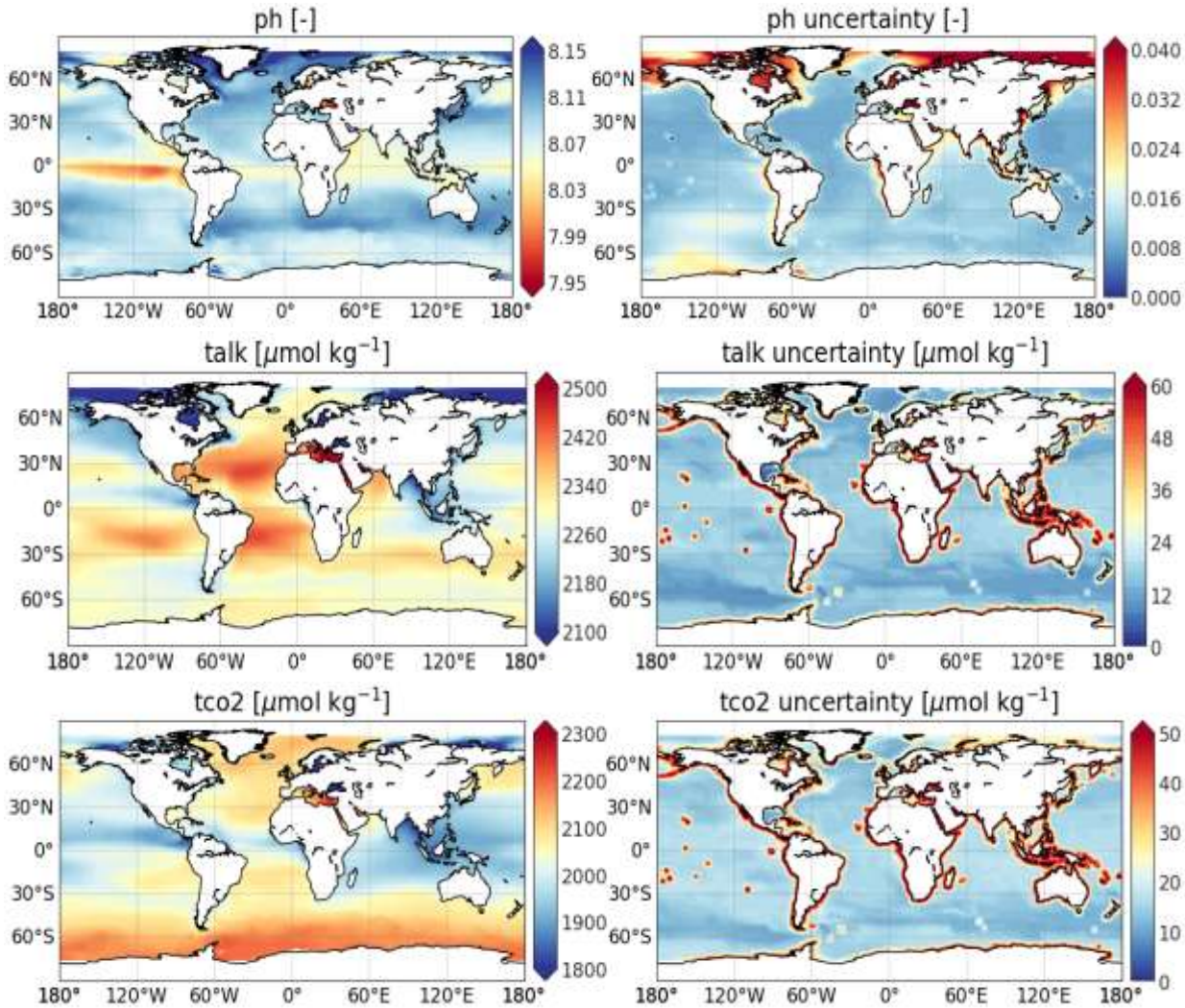

*Figure 7. Reconstructed surface ocean pH averaged over the global ocean for 1985 to 2022. Temporal mean estimate (left) and uncertainty (right) computed for the 100-member ensemble of CMEMS-LSCE-FFNNv2 are shown. The uncertainty estimate per grid cell (1σ) is computed following Eq. (2). Spikes in the uncertainty maps of surface ocean alkalinity and DIC are traced back to the uncertainty field of the CMEMS salinity product (Table 2, **Copernicus Marine Data visualization tool for sea surface salinity error**).*

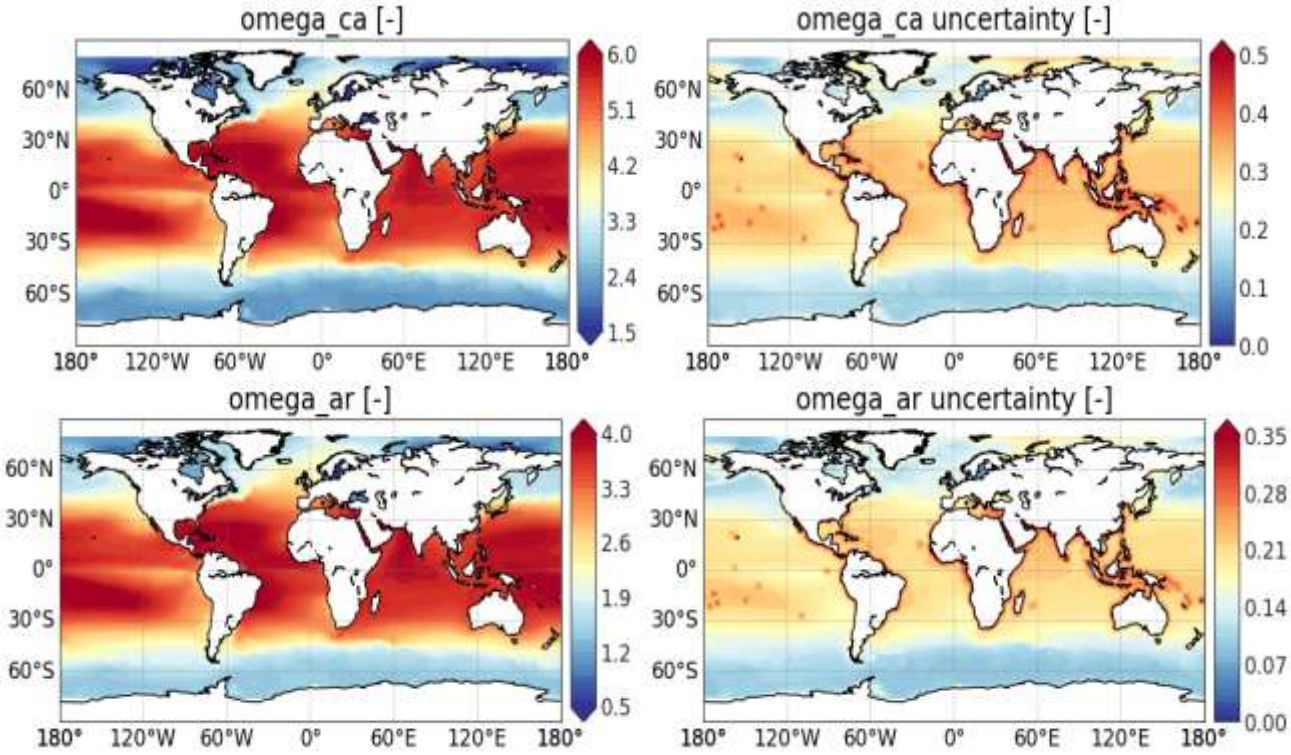

*Figure 8. Reconstructed surface ocean saturation state with respect to calcite (omega_ca) and aragonite (omega_ar) averaged over the global ocean for 1985 to 2022. Temporal mean estimate (left) and uncertainty (right) computed for the 100-member ensemble of CMEMS-LSCE-FFNNv2 are shown. The uncertainty estimate per grid cell (1σ) is computed following Eq. 2. Spikes in the uncertainty maps of surface ocean saturation state are traced back to the uncertainty field of the CMEMS salinity product (Table 2, **Copernicus Marine Data visualization tool for sea surface salinity error**).*

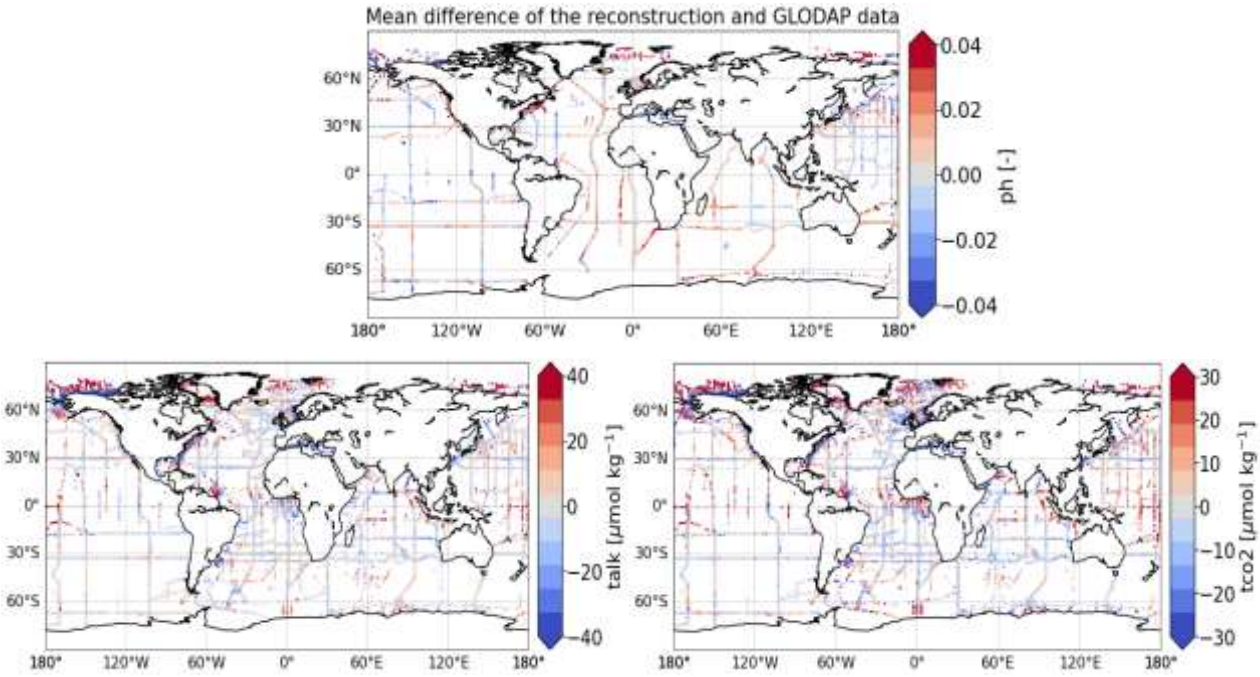

Figure 9. Maps of the mean of the differences between MULTIOBS and GLODAPv2.2022 bottle dataset for total alkalinity (talk), DIC (tco2), and pH (ph).

V SYSTEM'S NOTICEABLE EVENTS, OUTAGES OR CHANGES

MULTIOBS_GLO_BIO_CARBON_SURFACE_REP_015_008 is the new name of MULTIOBS_GLO_BIO_REP_015_005.

The first release (in 2020) of the MULTIOBS_GLO_BIO_CARBON_SURFACE_REP_015_008 product corresponds to a reprocessed and extended time series of monthly spco2, fgco2, ph over the global ocean at 1° spatial resolution. Estimates of spco2 are obtained from an ensemble of feed forward neural network (FFNNs) (Chau et al. 2022). It is referred to as CMEMS-LSCE-FFNNv2 and it is an improvement (method-wise) of the 1st version (LSCE-FFNN-v1) described in Denvil-Sommer et al. (2019), see Chau et al. (2020) for intercomparison. All variables are distributed with associated uncertainties derived from the 100-member ensemble.

Since the year 2021, the full CMEMS-LSCE-FFNN product including data over the coasts and high latitudes (above 60°N) has been submitted to CMEMS (and Global Carbon Project). Due to these changes, all statistics reported in the current document are significantly different from those in the previous version (2020). Note that the larger errors are derived from the reconstruction over the coasts and high latitudes.

Since the year 2022, time series of the 4 new variables (surface ocean alkalinity, dissolved inorganic carbon, saturation state with respect to calcite and aragonite) and associated reconstruction uncertainties have been provided. See Section IV for further updates of the evaluation corresponding to this release.

The year 2023 marks the first release of CMEMS-LSCE datasets of the seven carbonate system variables at monthly, 0.25° resolutions. A full data assessment is presented in Chau et al, (2023).

VI QUALITY CHANGES SINCE PREVIOUS VERSION

This new release CMEMS-LSCE (v2023) is an upgraded version of the previous (v2022) by increasing spatial resolution from 1° to 0.25°. The following results illustrate the comparison between the two versions focusing on data evaluation of spco2 (1° and 0.25°).

Skill scores of CMEMS-LSCE (v2023), and the previous version are reported in Table 6 for spco2. The two models share similar skill scores over the open ocean as expected. In the coastal sector, the higher resolution marginally improves spco2 reconstruction. The two FFNN reconstructions (0.25° and 1°) share similarities in overall structures of pCO2 over the coastal-open-ocean continuum (Figure 9). However, the higher spatial resolution outperforms its lower resolution counterpart in reproducing fine-scale features of pCO2 in the transition from nearshore regions to the adjacent open ocean. The increase in model spatial resolution translates into a greater spatial coverage of the continental shelves and thus an increase in the amount of data over the coastal domain. Results comparing the two FFNN models at coastal observing stations of spco2 highlight that the 0.25°-resolution model performs better in reproducing seasonality to interannual variations of spco2 observations (see Figure 5 and further analysis in Chau et al. 2023).

The two versions are consistent in terms of monthly global means of spco2 and pH and the monthly integration of air-sea fluxes of CO2 (Figure 10).

Table 6: Comparison between CMEMS-LSCE-FFNNv2 versions released in 2022 and 2023 for reconstruction of surface ocean spco2 over the period 1985-2021. The assessment is on spco2 values from SOCAT data that are not used during algorithm training. Global statistics over the 5 ocean basins (Figure 3) are computed with SOCATv2023.

Basins	RMSD (µatm)				r^2			
	Open		Coastal		Open		Coastal	
	v2022	v2023	v2022	v2023	v2022	v2023	v2022	v2023
Global	14.3	14.1	28.6	27.6	0.83	0.83	0.72	0.74
Arctic	28.5	29.0	43.2	42.4	0.69	0.66	0.52	0.54
Atlantic	13.7	13.5	26.0	25.1	0.81	0.82	0.77	0.78
Pacific	14.6	14.3	29.1	28.3	0.85	0.85	0.68	0.70
Indian Ocean	10.3	10.2	26.5	25.5	0.89	0.89	0.65	0.68
Southern Ocean	14.4	14.3	28.9	27.6	0.69	0.69	0.60	0.63

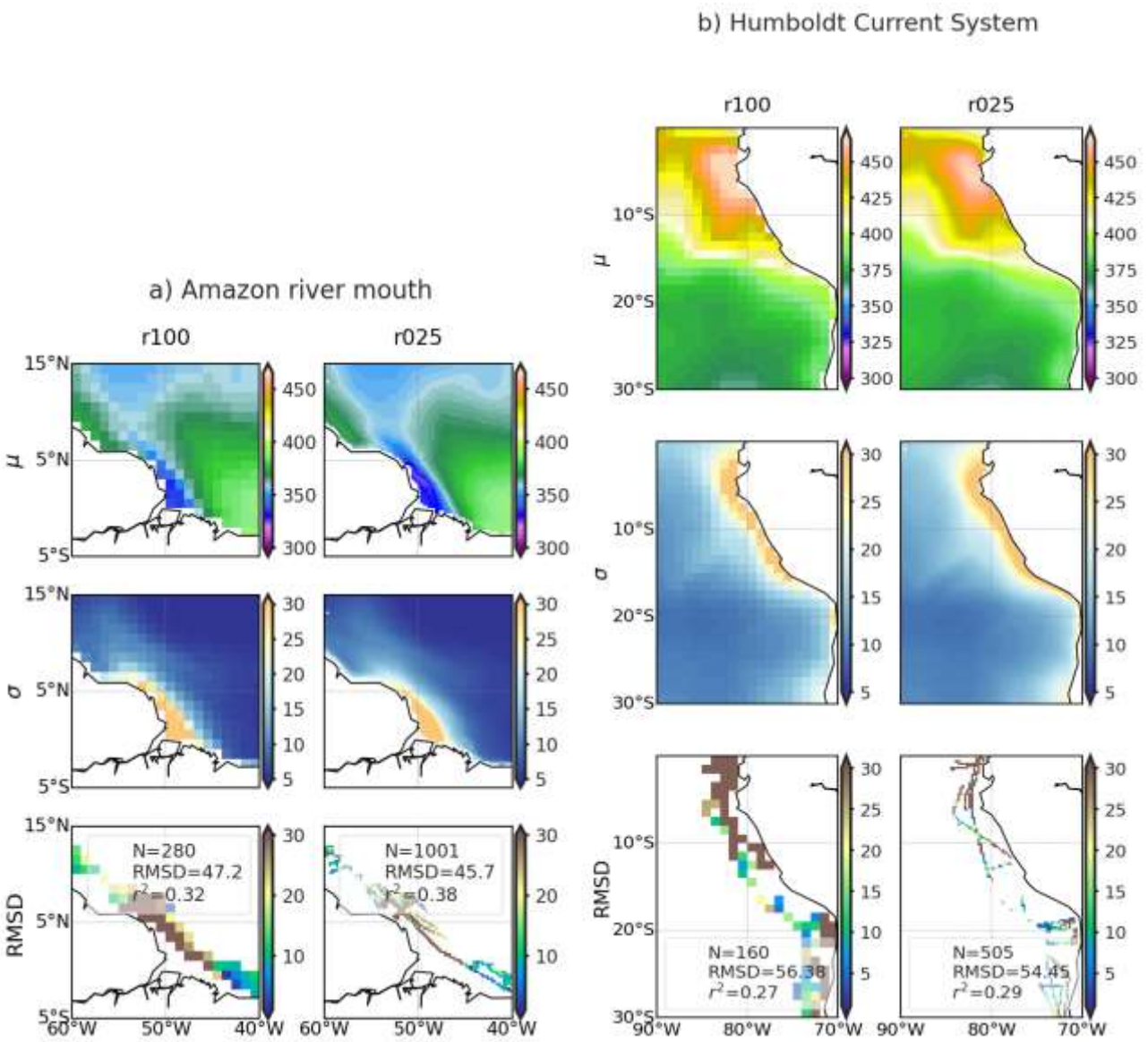

Figure 9. Comparison of CMEMS-LSCE-FFNN mapping spco2 at 1° (r100) and 0.25°(r025) resolutions over the mouth of the river Amazon (a) and the Humboldt Current System, western coast of South America (b). Spatial distributions of temporal mean spco2 (μ) and uncertainty (σ) estimates, and coastal-ocean RMSD are shown. Metrics present in the legend for each of the 3rd row include the number of coastal-ocean data (N) and RMSD are computed with coastal SOCAT data (Source: Chau et al. 2023).

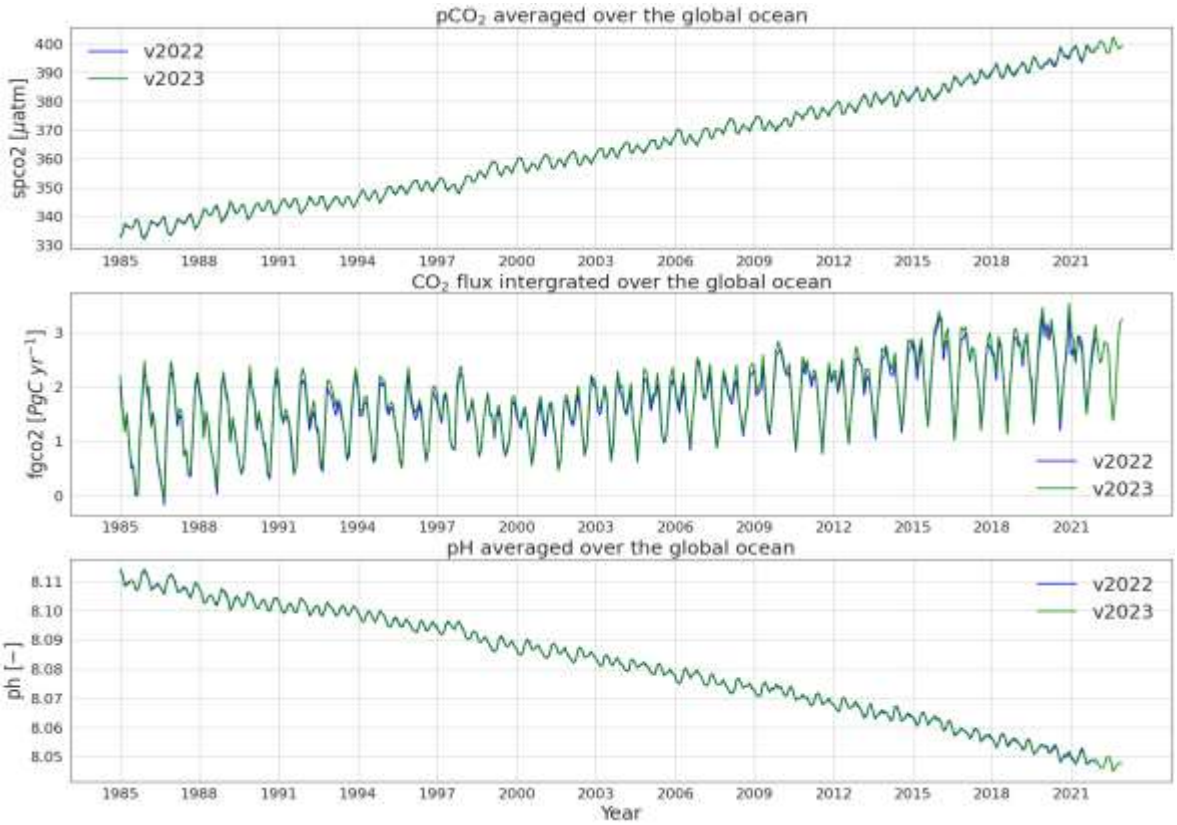

Figure 10. Global mean monthly surface ocean carbon dioxide partial pressure spco2 (top), monthly integration of air-sea fluxes fgco2 (middle), and global mean monthly pH (bottom) estimated by CMEMS-LSCE-FFNNv2 (2022, 2023).

VII REFERENCES

Bakker, D. C. E., Pfeil, B., Landa, C. S., Metzl, N., O'Brien, K. M., Olsen, A., Smith, K., Cosca, C., Harasawa, S., Jones, S. D., Nakaoka, S.-I. et al.: A multi-decade record of high-quality fCO2 data in version 3 of the Surface Ocean CO2 Atlas (SOCAT), Earth Syst. Sci. Data, 8, 383–413, https://doi.org/10.5194/essd-8-383-2016, 2016.

Bakker, D., Alin, S., Becker, M., Bittig, H., Castaño-Primo, R., Feely, R. A., Gritzalis, T., Kadono, K., Kozyr, A., Lauvset, S. K., Metzl, N., Munro, D., Nakaoka, S.-i., Nojiri, Y., O'Brien, K., Olsen, A., Pfeil, B., Pierrot, D., Steinhoff, T., Sullivan, K., Sutton, A., Sweeney, C., Tilbrook, B., Wada13, C., Wanninkhof, R., Wranne, A. W., et al.: SOCAT version 2023 for quantification of ocean CO2 uptake, DOI: 10.25921/r7xa-bt92, 2023.

Buongiorno Nardelli, B., R. Droghei, and R. Santoleri, 2016: Multi-dimensional interpolation of SMOS sea surface salinity with surface temperature and in situ salinity data. Rem. Sens. Environ., doi:10.1016/j.rse.2015.12.052.

Carter, B. R., Williams, N. L., Gray, A. R., & Feely, R. A.: Locally interpolated alkalinity regression for global alkalinity estimation. Limnology and Oceanography: Methods, 14(4), 268-277, 2016.

Carter, B. R., Feely, R. A., Williams, N. L., Dickson, A. G., Fong, M. B., & Takeshita, Y.: Updated methods for global locally interpolated estimation of alkalinity, pH, and nitrate. Limnology and Oceanography: Methods, 16(2), 119-131, 2018.

Chau, T. T. T., Gehlen, M., and Chevallier, F.: Global Ocean Surface Carbon Product. [Research Report] LSCE, https://hal.science/hal-02957656v1, 2020

Chau, T. T. T., Gehlen, M., and Chevallier, F.: A seamless ensemble-based reconstruction of surface ocean pCO_2 and air–sea CO_2 fluxes over the global coastal and open oceans, Biogeosciences, 19, 1087–1109, https://doi.org/10.5194/bg-19-1087-2022, 2022.

Chau, T. T. T., Gehlen, M., Metzl, N. and Chevallier, F.: CMEMS-LSCE: A global 0.25-degree, monthly reconstruction of the surface ocean carbonate system, Earth Syst. Sci. Data Discuss., https://doi.org/10.5194/essd-2023-146, in revision, 2023.

Chevallier, F., M. Fisher, P. Peylin, S. Serrar, P. Bousquet, F.-M. Bréon, A. Chédin, and P. Ciais, 2005: Inferring CO2 sources and sinks from satellite observations: method and application to TOVS data. J. Geophys. Res., 110, D24309, doi:10.1029/2005JD006390.

Chevallier, F., P. Ciais, T. J. Conway, T. Aalto, B. E. Anderson, P. Bousquet, E. G. Brunke, L. Ciattaglia, Y. Esaki, M. Fröhlich, A.J. Gomez, A.J. Gomez-Pelaez, L. Haszpra, P. Krummel, R. Langenfelds, M. Leuenberger, T. Machida, F. Maignan, H. Matsueda, J. A. Morguí, H. Mukai, T. Nakazawa, P. Peylin, M. Ramonet, L. Rivier, Y. Sawa, M. Schmidt, P. Steele, S. A. Vay, A. T. Vermeulen, S. Wofsy, D. Worthy, 2010: CO2 surface fluxes at grid point scale estimated from a global 21-year reanalysis of atmospheric measurements. J. Geophys. Res., 115, D21307, doi:10.1029/2010JD013887

Chevallier, F., 2013: On the parallelization of atmospheric inversions of CO2 surface fluxes within a variational framework. Geosci. Model. Dev., 6, 783-790, doi:10.5194/gmd-6-783-2013.

Denvil-Sommer, A., Gehlen, M., Vrac, M., and Mejia, C.: LSCE-FFNN-v1: a two-step neural network model for the reconstruction of surface ocean pCO_2 over the global ocean. Geoscientific Model Development, 12(5), 2091-2105, 2019.

Droghei, R., B. Buongiorno Nardelli, and R. Santoleri, 2016: Combining in-situ and satellite observations to retrieve salinity and density at the ocean surface. J. Atmos. Oceanic Technol. doi:10.1175/JTECH-D-15-0194.1.

Droghei, R., B. Buongiorno Nardelli, and R. Santoleri, 2018: A New Global Sea Surface Salinity and Density Dataset From Multivariate Observations (1993–2016), Front. Mar. Sci., 5(March), 1–13, doi:10.3389/fmars.2018.00084.

Fay, A.R., McKinley, G.A., and Lovenduski, N.S.: Southern Ocean carbon trends: Sensitivity to methods, Geophys. Res. Lett., 41, 6833–6840, doi:10.1002/2014GL061324, 2014.

Feely, R. A., Sabine, C. L., Takahashi, T., and Wanninkhof, R.: Uptake and storage of Carbon Dioxide in the ocean: the global CO_2 survey, Oceanography, 14, 18–32, https://doi.org/10.5670/oceanog.2001.03, 2001.

Feely, R.A., Wanninkhof, R., Takahashi, T. and Tans, P.: Influence of El Niño on the equatorial Pacific contribution to atmospheric CO2 accumulation. Nature, 398, 597-601.

Friedlingstein, P., O'Sullivan, M., Jones, M. W., Andrew, R. M., Gregor, L., Hauck, J., Le Quéré, C., Luijkx, I. T., Olsen, A., Peters, G. P., Peters, W., Pongratz, J., Schwingshackl, C., Sitch, S., Canadell, J. G., Ciais, P., Jackson, R. B., Alin, S. R., Alkama, R., Arneth, A., Arora, V. K., Bates, N. R., Becker, M., Bellouin, N., Bittig, H. C., Bopp, L., Chevallier, F., Chini, L. P., Cronin, M., Evans, W., Falk, S., Feely, R. A., Gasser, T., Gehlen, M., Gkritzalis, T., Gloege, L., Grassi, G., Gruber, N., Gürses, Ö., Harris, I., Hefner, M., Houghton, R. A., Hurtt, G. C., Iida, Y., Ilyina, T., Jain, A. K., Jersild, A., Kadono, K., Kato, E., Kennedy, D., Klein Goldewijk, K., Knauer, J., Korsbakken, J. I., Landschützer, P., Lefèvre, N., Lindsay, K., Liu, J., Liu, Z., Marland, G., Mayot, N., McGrath, M. J., Metzl, N., Monacci, N. M., Munro, D. R., Nakaoka, S.-I., Niwa, Y., O'Brien, K., Ono, T., Palmer, P. I., Pan, N., Pierrot, D., Pocock, K., Poulter, B., Resplandy, L., Robertson, E., Rödenbeck, C., Rodriguez, C., Rosan, T. M., Schwinger, J., Séférian, R., Shutler, J. D., Skjelvan, I., Steinhoff, T., Sun, Q., Sutton, A. J., Sweeney, C., Takao, S., Tanhua, T., Tans, P. P., Tian, X., Tian, H., Tilbrook, B., Tsujino, H., Tubiello, F., van der Werf, G. R., Walker, A. P., Wanninkhof, R., Whitehead, C., Willstrand Wranne, A., Wright, R., Yuan, W., Yue, C., Yue, X., Zaehle, S., Zeng, J., and Zheng, B.: Global Carbon Budget 2022, Earth Syst. Sci. Data, 14, 4811–4900, https://doi.org/10.5194/essd-14-4811-2022, 2022.

Garcia H.E., T.P. Boyer, O.K. Baranova, R.A. Locarnini, A.V. Mishonov, A. Grodsky, C.R. Paver, K.W. Weathers, I.V. Smolyar, J.R. Reagan, D. Seidov, M.M. Zweng (2019).

Gregor, L. and Gruber, N.: OceanSODA-ETHZ: a global gridded data set of the surface ocean carbonate system for seasonal to decadal studies of ocean acidification, Earth Syst. Sci. Data, 13, 777–808, https://doi.org/10.5194/essd-13-777-2021, 2021.

Good, S.; Fiedler, E.; Mao, C.; Martin, M.J.; Maycock, A.; Reid, R.; Roberts-Jones, J.; Searle, T.; Waters, J.; While, J.; Worsfold, M. The Current Configuration of the OSTIA System for Operational Production of Foundation Sea Surface Temperature and Ice Concentration Analyses. Remote Sens. 2020, 12, 720, doi:10.3390/rs12040720

Gurney, K., Baker D., Rayner, P. and Denning S.: Interannual variations in continental-scale net carbon exchange and sensitivity to observing networks estimated from atmospheric CO_2 inversions for the period 1980 to 2005. Global Biogeochemical Cycles, 22, GB3025, 2008.

Hauck J., Zeising M., Le Quere C., Gruber N., Bakker D. C., Bopp L., Chau T. T. T., Gürses O., Ilyina T., Landschützer P., Lenton A., Resplandy L., Rödenbeck C., Schwinger J., Se R.: Consistency and challenges in the ocean carbon sink estimate for the Global Carbon Budget, J. Front. Mar. Sci. - Ocean Observation, doi: 10.3389/fmars.2020.571720, 2020.

Hersbach, H., Bell, B., Berrisford, P., Biavati, G., Horányi, A., Muñoz Sabater, J., Nicolas, J., Peubey, C., Radu, R., Rozum, I., Schepers, D., Simmons, A., Soci, C., Dee, D., Thépaut, J-N. (2018): ERA5 hourly data on single levels from 1959 to present. Copernicus Climate Change Service (C3S) Climate Data Store (CDS). (Accessed on < DD-MMM-YYYY >), 10.24381/cds.adbb2d47

Iida, Y., Kojima, A., Takatani, Y., Nakano, T., Midorikawa, T., and Ishii, M.: Trends in pCO2 and sea-air CO2 flux over the global open oceans for the last two decades, J. Oceanogr., 71, 637–661, doi:10.1007/s10872-015-0306-4, 2015.

Landschützer, P., Gruber, N. and Bakker, D.C.E.: Decadal variations and trends of the global ocean carbon sink, Global Biogeochemical Cycles, 30, 1396-1417, doi:10.1002/2015GB005359, 2016

Landschützer, P., Gruber, N., Haumann, A., Rödenbeck, C., Bakker,D. C. E., van Heuven, S., Hoppema, M., Metzl, N., Sweeney, C.,Takahashi, T., Tilbrook, B., and Wanninkhof, R.: The reinvigo-ration of the Southern Ocean carbon sink, Science, 349, 1221–1224, https://doi.org/10.1126/science.aab2620, 2015.

Laruelle, G. G., Dürr, H. H., Lauerwald, R., Hartmann, J., Slomp,C. P., Goossens, N., and Regnier, P.: Global multi-scale segmen-tation of continental and coastal waters from the watersheds to the continental margins, Hydrol. Earth Syst. Sci., 17, 2029–2051, doi:10.5194/hess-17-2029-2013, 2013.

Laruelle, G. G., Landschützer, P., Gruber, N., Tison, J.-L., Delille, B., and Regnier, P.: Global high-resolution monthly pCO2 climatology for the coastal ocean derived from neural network interpolation, Biogeosciences, 14, 4545–4561, 2017.

Lauvset, S. K., Lange, N., Tanhua, T., Bittig, H. C., Olsen, A., Kozyr, A., Alin, S., Álvarez, M., Azetsu-Scott, K., Barbero, L., Becker, S., Brown, P. J., Carter, B. R., da Cunha, L. C., Feely, R. A., Hoppema, M., Humphreys, M. P., Ishii, M., Jeansson, E., Jiang, L.-Q., Jones, S. D., Lo Monaco, C., Murata, A., Müller, J. D., Pérez, F. F., Pfeil, B., Schirnick, C., Steinfeldt, R., Suzuki, T., Tilbrook, B., Ulfsbo, A., Velo, A., Woosley, R. J., and Key, R. M.: GLODAPv2.2022: the latest version of the global interior ocean biogeochemical data product, Earth System Science Data, 14, 5543–5572, https://doi.org/10.5194/essd-14-5543-2022, 2022.

Lewis, E., Wallace, D., & Allison, L. J.: Program developed for CO2 system calculations (No. ORNL/CDIAC-105). Brookhaven National Lab., Dept. of Applied Science, Upton, NY (United States); Oak Ridge National Lab., Carbon Dioxide Information Analysis Center, TN (United States), 1998.

Menemenlis, D., Campin, J., Heimbach, P., Hill, C., Lee, T., Nguyen, A., Schodlok, M., and Zhang, H.: ECCO2: High resolution global ocean and sea ice data synthesis, Mercator Ocean, Quarterly Newsletter, 31, 13–21, 2008.

Orr, J.C., J.-M. Epitalon, A. G. Dickson, and J.-P. Gattuso (2018) Routine uncertainty propagation for the marine carbon dioxide system, in prep. for Mar. Chem., in press, http: s://doi.org/10.1016/j.marchem.2018.10.006.

Regnier, P., Resplandy, L., Najjar, R. G., and Ciais, P.: The land-to-ocean loops of the global carbon cycle, Nature, 603, 401–410, https://doi.org/10.1038/s41586-021-04339-9, 2022.

Rödenbeck, C., Bakker, D. C. E., Metzl, N., Olsen, A., Sabine, C., Cassar, N., Reum, F., Keeling, R. F., and Heimann, M.: Interannual sea-air CO2 flux variability from an observation-driven ocean mixed-layer scheme, Biogeosciences, 11, 4599–4613, doi:10.5194/bg-11-4599-2014, 2014.

Rödenbeck, C., Bakker, D. C. E., Gruber, N., Iida, Y., Jacobson, A. R., Jones, S., Landschützer, P. et al.: Data-based estimates of the ocean carbon sink variability—first results of the Surface Ocean pCO2 Mapping intercomparison (SOCOM), Biogeosciences, 12, 7251–7278, https://doi.org/10.5194/bg-12-7251-2015, 2015.

Takahashi, T., Sutherland, S.C., Wanninkhof, R., Sweeney, C., Feely, R.A., Chipman, D.W., Hales, B., Friederich, G., Chavez, F., Sabine, C., et al.: Climatological mean and decadal change in surface ocean pCO2, and net sea-air CO2 flux over the global oceans, Deep.-Sea Res. II, 56(8–10), 554–577, https://doi.org/10.1016/j.dsr2.2008.12.009, 2009.

van Heuven, S. M., Hoppema, M., Huhn, O., Slagter, H. A., & de Baar, H. J.: Direct observation of increasing CO2 in the Weddell Gyre along the Prime Meridian during 1973–2008. Deep Sea Research Part II: Topical Studies in Oceanography, 58(25-26), 2613-2635, 2011.

Wanninkhof, R.: Relationship between wind speed and gas exchange over the ocean revisited, *Limnol. Oceanogr. Methods*, 12, doi:10.4319/lom.2014.12.351, 2014.

Weiss, R.: Carbon dioxide in water and seawater: the solubility of a non-ideal gas, Mar. Chem., 2, 203–205, https://doi.org/10.1016/0304-4203(74)90015-2, 1974.